Horný, L., Chlup, H., Kužma, J., Růžička, P., 2022. Inflation-extension behaviour of 3D printed elastomer tubes and their constitutive description. Bioprinting 25, e00192. Manuscript version. Link to the publisher version: https://doi.org/10.1016/j.bprint.2022.e00192.

Inflation-extension behaviour of 3D printed elastomer tubes and their constitutive description

Lukáš Horný[1#], Hynek Chlup[1], Ján Kužma[1], Pavel Růžička[1]

[1] Czech Technical University in Prague, Faculty of Mechanical Engineering, Technická 4, 160 00, Prague, Czech Republic
[#] Corresponding author: Lukáš Horný, lukas.horny@fs.cvut.cz

Abstract: It is known that arteries in situ are axially prestretched. This can be proved during an autopsy when a cylindrical segment of an artery is removed from a body. The segment retracts to ex situ length, and the ratio of in situ length to ex situ length defines the amount of prestretching. Ex vivo inflation-extension experiments showed that axial prestretching is advantageous from a mechanical point of view because it minimizes the longitudinal movement of an artery during pressure pulse transmission. Furthermore, calculations suggested that axial prestretching decreases variation of axial stress and makes the radial distension of arteries easier. Recently, it has been shown theoretically that axial prestretching of a nonlinear tube increases the volume, which it is able to accommodate during pressurization. The present study complements previous results with the experimental observation of this fact. Tango Plus tubes, made with the help of 3D printing PolyJet technology, were cyclically pressurized. Axial prestretching was induced by hanging weights on the vertically oriented tubes. The results showed that the internal volume of the tubes increased with the elevated axial prestretch. The recorded mechanical responses were utilized in the regression analysis to identify the material parameters of the tubes. It was found that the hyperelastic Ogden model is suitable for describing the mechanical behaviour of the Tango Plus material. Our study demonstrates that 3D printing can be used to produce tubes, which, for example, may serve as a substitute for biological tissues in laboratory experiments. Simultaneously, this study yields the constitutive parameters of the digital material identified at multiaxial stress conditions. Such parameters are necessary, for instance, in the finite element analyses of parts undergoing loading conditions which result in multiaxial stress states.

Keywords: Additive manufacturing, axial prestretch, constitutive model, digital material, hyperelastic material, pressurization.

1. Introduction

It is known that arteries in situ are axially prestretched (Bergel 1961; Dobrin and Doyle, 1970; Han and Fung, 1995). This can be proved during surgical resection or in autopsy, when a cylindrical segment of an artery is removed from a body (Horný et al., 2011, 2014a, 2017). The segment retracts to its ex situ length, and the ratio of in situ length to ex situ length defines the amount of prestretching. Ex vivo inflation-extension experiments with human as well as with animal arteries showed that axial prestretching is advantageous from a mechanical point of view, because it minimizes the longitudinal movement of an artery during pressure pulse transmission (Van Loon et al., 1977; Schulze-Bauer et al., 2003; Sommer et al., 2010; Kamenskiy et al., 2016). Computational simulations suggest that axial prestretching decreases variation of axial stress in the arterial wall (Horný et al., 2014b).

Possibly more interesting than the relationship between longitudinal movement and changes in axial force, or axial stress, is the effect which axial prestretch has on the radial distension of the tube itself. Studies by Horný et al. (2014b), and Horný and Netušil (2016) showed that an axially prestretched tube exhibits higher distensibility, and confirmed that this effect is associated with geometrical and material nonlinearity, and it completely vanishes within the framework of the linear elasticity. The very recent paper by Horný and Petřivý (2020) has moreover shown that it is not only variation of the circumferential deformation which increases due to axial prestretching, but also the total internal volume, which the artery accommodates through pressurization, is increased in longitudinally prestretched tubes.

These results were obtained through theoretical examination of the mechanics of hyperelastic thin-walled tubes and demonstrated in computer simulations of the inflation-extension behaviour. However, experiments showing how longitudinal prestretch changes the internal volume of pressurized tubes are lacking in the literature. This is the main goal of the present study.

It is advantageous to work with artificial substitutes of tissues in the early phase of medical engineering development (Salman et al., 2019). Arterial phantoms made from industrial materials usually exhibit lesser heterogeneity in their internal structure, which reduces the variance of measured quantities. Research focused on the pressure pulse wave transmission (Balocco et al., 2010; Chee et al., 2016), stent deployment simulations (Azarnoush et al., 2019), or in vitro phantoms for ultrasound-based constitutive parameters identification (Lopata et al., 2009; Chayer et al., 2019) can be cited as examples.

One possible way to create such tubes would be rapid prototyping based on additive technologies. There are some 3D printing methods enabling the production of compliant parts. Typically, they are based on photo-polymers, which resemble elastomer behaviour. The tubes used in our inflation-extension experiments were obtained with the help of PolyJet technology. The digital material from which they were built is based on Tango Plus supplied by Stratasys.

With the expanding use of 3D printing, the need for suitable constitutive models for digital materials is growing. Studies focused on the fully nonlinear constitutive characterization of the Tango Plus material are rather rare in the literature. Moreover, they are usually based on uniaxial tension experiments (Mańkowski and Lipnicki 2017; Slesaremko and Rudykh 2018; Ryu et al., 2019; Meng et al., 2020). Studies engaging other experimental methods are sporadic at present. Our survey has found only a few very recent studies by Pagac et al. (2020; uniaxial and volumetric compression constitutive characterization), Abayazid and Ghajari (2020; uniaxial tension and compression), and Morris et al. (2019; uniaxial and planar biaxial tensile testing).

Hence, the second goal of our work is to complete our knowledge of Tango Plus material with the parameters of the constitutive model, which were identified in experiments inducing multiaxial stress conditions in the tested samples.

2. Materials and Methods

2.1 Samples

The tubes were manufactured by means of 3D printing based on PolyJet technology in Stratasys J750 (Stratasys, USA). The tubes' material was purchased from Staratasys and is traded under the name Tango Plus. Tango is offered as a material intended for the production of parts conventionally manufactured from rubber-like materials. PolyJet 3D printing works by jetting layers of a liquid photopolymer, which are instantly cured with UV light. Tango is a commercial label for a whole family of rubber simulating-materials. Our tubes were printed from Tango Plus based materials, denoted as FLX930 and FLX9940. FLX930 represents pure Tango Plus, whereas FLX9940 is created as a digital material by adding Vero Clear RGD810 (acrylic thermoplastic) into Tango Plus FLX930.

All the tubes were printed with the same dimensions. They had a cylindrical body with an inner radius of R_i = 5 mm, and a wall thickness H = 1.4 mm. The length of the body was 100 mm. The cylindrical body of each tube was continued with a slightly conical connecting part to make mounting into the experimental setup easier. The conical ends had a length of 20 mm so that the total length of the tube was 140 mm. At the conical part of the tube, the inner radius of the tube was steadily increased from 5 mm to 5.4 mm, whereas the outer radius of the tube was R_o = 6.4 mm along its entire length.

2.2 Experimental setup and inflation-extension protocol

Figure 1 displays the experimental setup, developed in-house, which was used in the pressurization experiments. It consists of a basic frame with the measuring chamber into which the tube is mounted. In the course of the experiment, the tube is oriented vertically, and at its lower end is a weight which induces axial prestretch, hanging on tube's plug (Figure 1A). During pressurization, a deformed geometry was recorded by two digital cameras, Basler acA2500 (2592x1944 px., 5 MB; Basler, Germany). They were arranged to record the experimental scene from mutually perpendicular points of view. Recordings were taken at a frame rate of 5 Hz. In the post-processing, the deformation of a sample was determined by an image analysis of the recorded photos. The image analysis script was based on the edge detection algorithm and was programmed in Matlab. The inflation pressure was measured with the help of a pressure transducer, KTS Cressto (Cressto, Czech Republic), and consequently the signal was digitized by NI USB-6289 (18-bit; National Instruments, USA), and recorded onto a PC at a sampling frequency of 100 Hz.

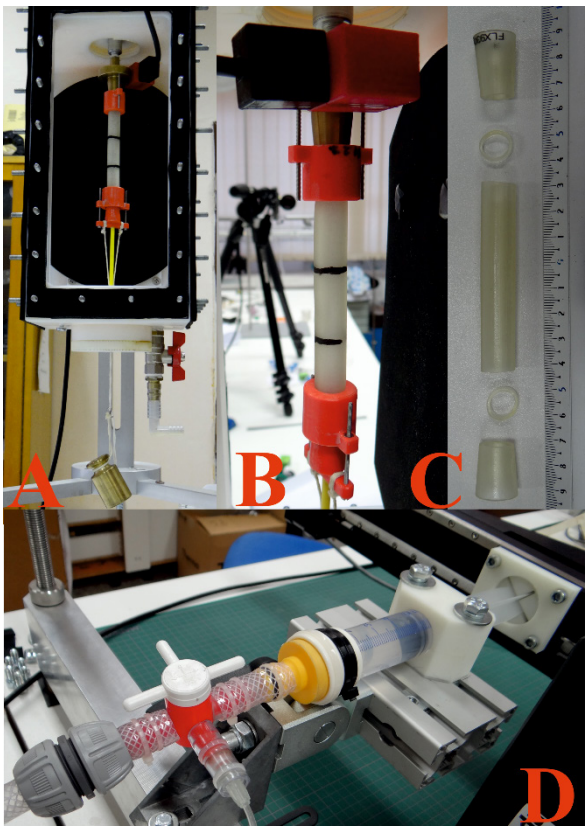

Figure 1. Inflation-extension setup. A – Measuring chamber with mounted tube and hanging weight. B – Detail of the mounted sample with connected pressure transducer and a camera in the background. C – The sample detached from the setup after the experimental protocol was completed. D – pressure generator consisting from PC-controlled stepper motor, cylinder and piston.

Pressure loading was induced by a programmable stepper motor, 8MT295 (Standa, Lithuania), which pushed onto the piston (Figure 1D). The piston underwent a slow translational movement, which induced a quasi-static cyclic pressurization with a triangular waveform. Each measuring sequence consisted of four loading-unloading cycles. Samples consecutively underwent measuring sequences with a suspended weight of a mass equal to 0, 130, 260, and 390 g.

2.3 Identification of material parameters and comparison of materials

It was assumed that the mechanical response of 3D-printed tubes recorded during the inflation-extension experiments corresponds to the behaviour of incompressible hyperelastic material. The constitutive equation of such a material can be written in the form of (1). Here W denotes the elastic potential commonly referred to as the strain energy density function, $\boldsymbol{\sigma}$ is the Cauchy stress tensor, $\mathbf{I}$ denotes the second order unit tensor, and p is the undetermined multiplier introducing hydrostatic stress into the constitutive equation, because this component of $\boldsymbol{\sigma}$ cannot be derived from W due to incompressibility.

$$\boldsymbol{\sigma} = \frac{\partial W}{\partial \mathbf{F}}\mathbf{F}^T - p\mathbf{I} \tag{1}$$

Symbol $\mathbf{F}$ in (1) denotes the deformation gradient tensor. Consider a material particle, which in the reference position $\boldsymbol{X}$ has polar cylindrical coordinates (R,Θ,Z), whereas in the deformed position $\boldsymbol{x}$ it has polar cylindrical coordinates (r,θ,z). We assumed that the inflation-extension behaviour of our tubes can be described by kinematics expressed in (2).

$$h = \lambda_R H \qquad r = \lambda_\Theta R \qquad z = \lambda_Z Z \tag{2}$$

Here H and h respectively denote the thickness of the tube in the reference and deformed configuration. Under these conditions, $\mathbf{F}$ has the form $\mathbf{F} = diag[\lambda_R,\lambda_\Theta,\lambda_Z]$, and λ_K ($K = R, \Theta, Z$) play the role of principal stretches. Since the material is incompressible, $\lambda_R\lambda_\Theta\lambda_Z = 1$ holds.

According to Horný and Petřivý (2020), the internal pressure P and the force induced by the suspended weight F_{red} can, in case of an incompressible hyperelastic thin-walled tube, be expressed by equations (3) and (4). Here $\hat{W}$ denotes W with λ_R substituted from incompressibility condition, $\lambda_R = 1/(\lambda_\Theta\lambda_Z)$, and $\varepsilon = H/R_i$.

$$P = \frac{\varepsilon}{\lambda_\Theta\lambda_Z}\frac{\partial \hat{W}}{\partial \lambda_\Theta} \tag{3}$$

$$F_{red} = \varepsilon\pi R_i^2\left(2\lambda_Z\frac{\partial \hat{W}}{\partial \lambda_Z} - \frac{\lambda_\Theta}{\lambda_Z}\frac{\partial \hat{W}}{\partial \lambda_\Theta}\right) \tag{4}$$

In the last seventy years, many models of W have been developed. One of the most successful is that suggested by R. Ogden in 1972 (Ogden 1972, 1997). Its particular form is expressed in (5). In (5a) μ_k and α_k are material parameters which have to satisfy inequality (5b).

$$W = \sum_{k=1}^{N}\frac{\mu_k}{\alpha_k}\left(\lambda_R^{\alpha_k} + \lambda_\Theta^{\alpha_k} + \lambda_Z^{\alpha_k} - 3\right) \qquad \sum_{k=1}^{N}\alpha_k\mu_k > 0 \tag{5}$$

This model of strain energy was used to fit the inflation-extension response of Tango tubes. For the sake of simplicity, $N = 1$ was chosen. As a direct consequence, the denotation $\alpha_k = \alpha$ and $\mu_k = \mu$ is used in what follows.
Parameters α and μ were estimated by means of the least square optimization procedure, programmed in Maple 2020 with the help of NLPSolve command (nonlinear program solution). Objective function Q had the form given in (6). Here P^{EXP} and F^{EXP} denote directly measured internal pressure and reduced axial force, whereas P^{MOD} and F^{MOD} are their counterparts, predicted by means of (3) and (4). Weighting coefficients are denoted w_P and w_F and their initial estimates were equal to the inverse of the square of measured mean value.

$$Q = \sum_{i=1}^{n} \left(w_P \left(P_i^{EXP} - P_i^{MOD} \right)^2 + w_F \left(F_i^{EXP} - F_i^{MOD} \right)^2 \right) \tag{6}$$

To make the comparison of the mechanical behaviour of FLX930 and FLX9940 relatively easy, it was based on the stress in the uniaxial tension predicted by the model (5) with α and μ substituted with values obtained in the regression analysis. Under conditions of uniaxial tension, mechanical stress corresponding to (5) is given by the equation (7). Here λ_1 is the stretch in the loading direction. By the differentiation of (7) at $\lambda_1 = 1$, one obtains the initial Young modulus E_{ini} which expresses material properties within the context of the infinitesimal strain elasticity. It holds that $E_{ini} = 3/2\alpha\mu$.

$$\sigma_1 = \mu\lambda_1^{\alpha} - \mu\lambda_1^{-\frac{\alpha}{2}} \tag{7}$$

Let's finally note that the internal volume of the pressurized tube which follows the kinematics described by (2) is given by $\pi r_i^2 l$ where l is its current length. In such a case, the change of volume can be expressed as the ratio of current to reference volume and is given as $v = (\pi r_i^2 l)/(\pi R_i^2 L) = \lambda_\Theta^2 \lambda_Z$. In what follows, this quantity is used to evaluate the effect of axial prestretch on the volume of pressurized tubes.

Readers interested in further details of the mechanical response of nonlinearly elastic tubes can consult, among others, Merodio and Ogden (2016), El Hamdaoui et al. (2014, 2018), Wang et al. (2019), or Desena-Galarza et al. (2021), where inflation-extension behaviour is studied with regard to material anisotropy and deformation stability.

3. Results and Discussion

In total eight tubes underwent cyclic inflation-extension testing. They were printed from Tango material in a 3D printer, Stratasys J750, using PolyJet technology. Four of them were printed from FLX930 and the other four from a FLX9940 cartridge. Tubes were longitudinally prestretched by hanging a weight. Four values of the reduced axial force were applied within the testing, $F_{red} = 0$, 1.3, 2.6, and 3.9 N (let us remember that F_{red} is the force corresponding to the mass of the suspended weight). Four pressurization cycles were carried out with each axial load. The experiment was conducted as quasi-static loading and each pressurization cycle lasted for 25 s.

Figure 2 depicts the typical records obtained during experiments. Loading pressure P, circumferential stretch λ_Θ, axial stretch λ_Z, and relative volume v are here displayed as functions of time. The first loading cycle is represented with solid curves, whereas the fourth cycle is depicted with circles. The specific axial weight is highlighted with a colour. Figure 2 clearly suggests that there are minimal differences between the responses in the first cycle and in the fourth cycle.

A similar conclusion can be drawn from Figure 3, which displays the same quantities in the same cycles but with time being eliminated. Figure 3 moreover shows that areas bordered by loading and unloading

curves, which correspond to dissipated energy, are small and in the fourth cycle they are technically negligible. It suggests that Tango can be modelled as an elastic material. This conclusion is in accordance with previously published results obtained by Mańkowski and Lipnicki (2017), Ryu et al. (2019), Morris et al. (2020), and Meng et al. (2020).

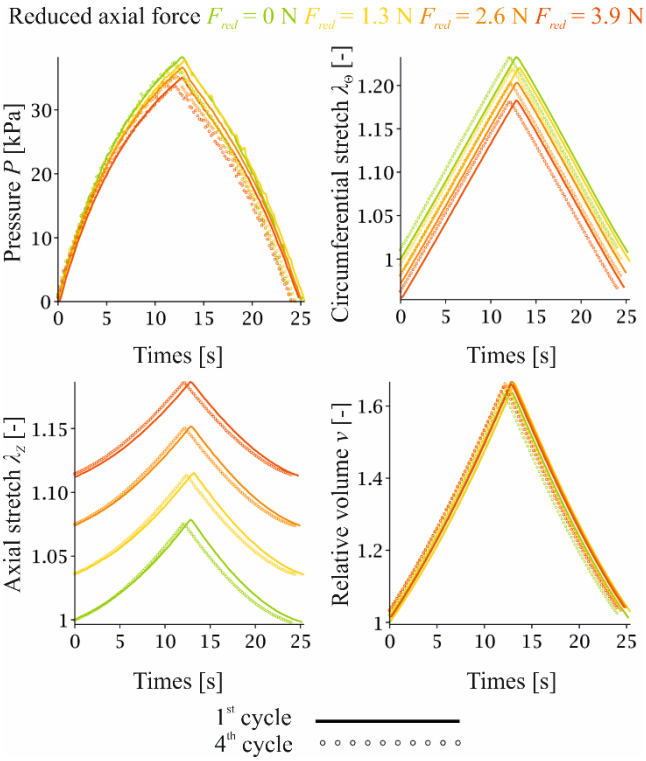

Figure 2. Time course of the inflation-extension response in the first and fourth loading cycle at each longitudinal weight.

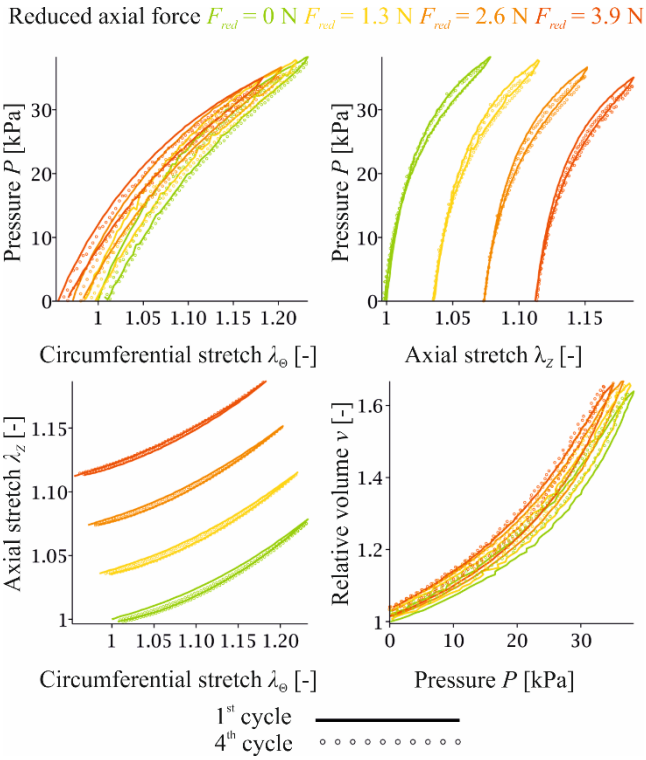

Figure 3. Inflation-extension response in the first and fourth loading cycle at each longitudinal weight. Results suggest that viscoelastic effects causing differences between loading and unloading, and between the first and the fourth cycle are rather small.

P–λ_Θ and P–λ_Z relationships depicted in Figure 3 document that Tango Plus sustained large deformations within our experiments and that its response is nonlinear. However, in contrast to known responses for arteries and veins, Tango Plus did not exhibit large strain stiffening within inflation-extension testing, which is in accordance with the behaviour of rubber-like tubes discussed in Holzapfel (2005).

Figure 3 also demonstrates the effect of axial pre-load. P–λ_Z panel shows the initial values of the axial stretch, i.e. the axial prestretch, which the tube sustained at $P = 0$. Within the range of our observation, tubes did not exhibit axial inversion, that is a transition from pressure-induced elongation to pressure-induced shortening (for further details see e.g. Horný and Petřivý, 2020). Our experiments confirm previous theoretical conclusion that the axial prestretching can decrease circumferential stiffness of pressurized tubes, which means that their radial distension is easier (Horný et al., 2014b; Horný and Netušil, 2016; Voňavková and Horný, 2020). This is clear from P–λ_Θ in Figure 3. One can recognize it when considering slopes of tangents made to curves at a given P.

The effect of axial prestretch on the internal volume of tubes is presented in P–v panel in Figure 3 and in detail in Figure 4. The order of the curves in the figures proves that axial prestretching increases the volume pushed into the tube. This effect has been theoretically discussed in Horný and Netušil (2016) and in Horný and Petřivý (2020) but without experimental confirmation. This property can be utilised in the design of cylindrical pumps working with compliant chambers. Note that this property can also be interpreted from a mechanical work point of view. The mechanical response presented in Figure 4 shows that if a constant volume is pushed into the compliant tube, the axially prestretched tube performs lower work during the working cycle than a non-prestretched tube. Considering that the heart ejects approximately constant volume during the systole, it follows that an axially prestretched aorta is capable of performing its blood accommodation function at a lower pressure than non-prestretched aorta.

The second goal of our study was to find a suitable constitutive description for FLX930 and FLX9940. The results presented in Figure 2 and 3 justify our decision to neglect the viscoelastic effects in the mechanical response of Tango. Figure 5 displays typical predictions of hyperelastic model (5) obtained with the help of a thin-walled approximation expressed in equations (3) and (4). Considering the Figure 5, one sees that in general the model fits well with the observation, although it is clear that it is more successful in pressure than in force predictions. A good agreement between the model and the observation is also expressed by the values of the coefficient of determination R^2 computed separately for predicted pressure and force (see Figure 5). On the other hand, predictions associated with low levels of pressure deviate somewhat from observations. Table 1 contains predicted parameters and R^2 for all samples included in our study.

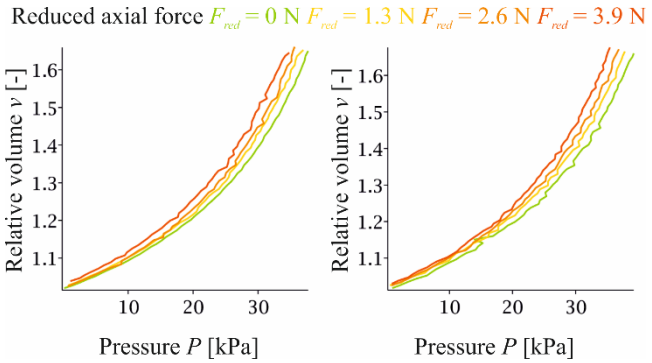

Figure 4. Effect of axial prestretch on the internal volume of pressurized tubes observed in two different samples. Axially prestretched tubes exhibit a higher accommodated volume than non-prestretched tubes. The figure depicts only loading parts of the response.

Table 1. Estimated material parameters

Material	μ [kPa]	α [-]	R_P^2	R_F^2	E_{ini} [kPa]
FLX9940	142.5	3.254	0.9953	0.9653	695.8
FLX9940	150.7	3.152	0.9960	0.9536	712.4
FLX9940	144.0	3.224	0.9944	0.9393	696.4
FLX9940*	119.8	4.021	0.9934	0.9705	722.4
FLX930	86.12	3.451	0.9796	0.9715	445.8
FLX930	99.04	3.095	0.9917	0.9175	459.8
FLX930	99.69	2.669	0.9251	0.9077	399.1
FLX930#	77.27	3.790	0.8918	-	439.3

*sample survived 3 levels of axial loading (0 g, 130 g, 260 g)
#sample survived only 1st level of axial loading (0 g)

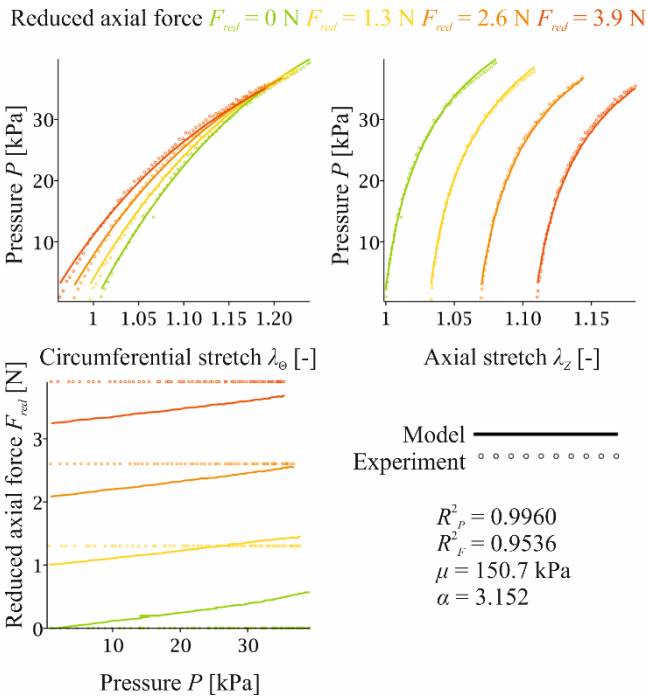

Figure 5. Comparison between observed inflation-extension response and the model (FLX9940, second row in Table 1).

Table 1 also contains slopes of the tangents made to the uniaxial tension responses at the beginning of the loading, E_{ini}, which correspond to the small strain Young modulus of elasticity. This quantity, hand in hand with Figure 6, which depicts predictions of uniaxial tensile response, is used to evaluate whether differences between FLX9940 and FLX930 exist. Both complete tensile response and E_{ini} suggest that FLX9940 is stiffer than FLX930. It is in accordance with the fact that Vero Clear represents hard material, and one should achieve stiffer polymer by adding them into compliant Tango Plus (Mańkowski and Lipnicki, 2017; Meng et al., 2020).

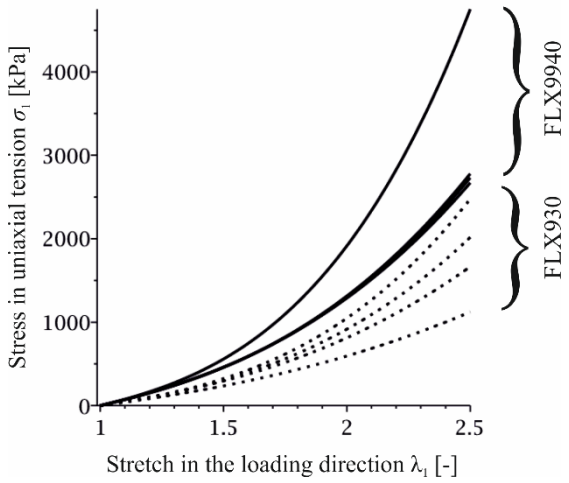

Figure 6. Comparison between identified models for FLX930 and FLX9940 in uniaxial tension.

Specific values of the material parameters μ and α in Table 1 also suggest that FLX9940 is stiffer than pure Tango Plus. On the other hand, the experimental records obtained in inflation-extension testing did not revealed any significant differences in the character of their mechanical response. Both materials manifested negligible viscoelasticity, a concave shape of P–λ_Θ and P–λ_Z relationships and confirmed an elevated internal volume during pressurization at axial prestretch.

Acknowledgement

This study has been supported by the Czech Science Foundation in project 18-26041S entitled “Effect of axial prestretch on the mechanical response of nonlinearly elastic and viscoelastic tubes”.

References

Abayazid, F. F., Ghajari, M., 2020. Material characterisation of additively manufactured elastomers at different strain rates and build orientations. Addit. Manuf. 33, 101160. http://doi.org/10.1016/j.addma.2020.101160.

Azarnoush, H., Pazos, V., Vergnole, S., Boulet, B., Lamouche, G., 2019. Intravascular optical coherence tomography to validate finite-element simulation of angioplasty balloon inflation. Phys. Med. Biol. 64, 095011. https://doi.org/10.1088/1361-6560/ab0d58.

Balocco, S., Basset, O., Courbebaisse, G., Boni, E., Frangi, A. F., Tortoli, P., Cachard, C., 2010. Estimation of the viscoelastic properties of vessel walls using a computational model and doppler ultrasound. Phys. Med. Biol. 55, 3557-3575. https://doi.org/10.1088/0031-9155/55/12/019.

Bergel, D. H., 1961. The static elastic properties of the arterial wall. J. Physiol. 156, 445-457. http://doi.org/10.1113/jphysiol.1961.sp006686.

Chayer, B., Van Den Hoven, M., Cardinal, M. – H. R., Li, H., Swillens, A., Lopata, R., Cloutier, G. (2019). Atherosclerotic carotid bifurcation phantoms with stenotic soft inclusions for ultrasound flow and vessel wall elastography imaging. Phys. Med. Biol. 64, 095025. https://doi.org/10.1088/1361-6560/ab1145.

Chee, A. J. Y., Ho, C. K., Yiu, B. Y. S., Yu, A. C. H., 2016. Walled carotid bifurcation phantoms for imaging investigations of vessel wall motion and blood flow dynamics. IEEE Trans. Ultrason. Ferroelectr. Freq. Control 63, 1852-1864. https://doi.org/10.1109/TUFFC.2016.2591946.

Desena-Galarza, D., Dehghani, H., Jha, N. K., Reinoso, J., Merodio, J., 2021. Computational bifurcation analysis for hyperelastic residually stressed tubes under combined inflation and extension and aneurysms in arterial tissue. Finite Elem. Anal. Des. 197 https://doi.org/10.1016/j.finel.2021.103636.

Dobrin, P. B., Doyle, J. M., 1970. Vascular smooth muscle and the anisotropy of dog carotid artery. Circ. Res. 27, 105-119. https://doi.org/10.1161/01.RES.27.1.105.

El Hamdaoui, M., Merodio, J., Ogden, R. W., Rodríguez, J., 2014. Finite elastic deformations of transversely isotropic circular cylindrical tubes. Int. J. Solids Struct. 51(5), 1188-1196. https://doi.org/10.1016/j.ijsolstr.2013.12.019.

El Hamdaoui, M., Merodio, J., Ogden, R. W., 2018. Deformation induced loss of ellipticity in an anisotropic circular cylindrical tube. J. Eng. Math. 109(1), 31-45. https://doi.org/10.1007/s10665-017-9904-z.

Han, H. - C., Fung, Y. - C., 1995. Longitudinal strain of canine and porcine aortas. J. Biomech. 28, 637-641. http://doi.org/10.1016/0021-9290(94)00091-H.

Holzapfel, G., 2005. Similarities between soft biological tissues and rubberlike materials, In: Constitutive Models for Rubber IV. A.A. Balkema , Leiden, pp. 607-617.

Horny, L., Adamek, T., Gultova, E., Zitny, R., Vesely, J., Chlup, H., Konvickova, S., 2011. Correlations between age, prestrain, diameter and atherosclerosis in the male abdominal aorta. J. Mechan. Behav. Biomed. Mater. 4, 2128-2132. https://doi.org/10.1016/j.jmbbm.2011.07.011.

Horny, L., Adamek, T., Kulvajtova, M., 2014a. Analysis of axial prestretch in the abdominal aorta with reference to post mortem interval and degree of atherosclerosis. J. Mechan. Behav. Biomed. Mater. 33, 93-98. http://doi.org/10.1016/j.jmbbm.2013.01.033.

Horný, L., Netušil, M., Voňavková, T., 2014b. Axial prestretch and circumferential distensibility in biomechanics of abdominal aorta. Biomech. Model. Mechanobiol. 13, 783-799. https://doi.org/10.1007/s10237-013-0534-8.

Horný, L., Netušil, M., 2016. How does axial prestretching change the mechanical response of nonlinearly elastic incompressible thin-walled tubes. Int. J. Mech. Sci. 106, 95-106. https://doi.org/10.1016/j.ijmecsci.2015.08.014.

Horný, L., Adámek, T., Kulvajtová, M., 2017. A comparison of age-related changes in axial prestretch in human carotid arteries and in human abdominal aorta. Biomech. Model. Mechanobiol. 16, 375-383. https://doi.org/10.1007/s10237-016-0797-y.

Horný, L., Petřivý, Z., 2020. Inversion point and internal volume of pressurized nonlinearly elastic tube. Int. J. Non-Lin. Mech. 125, 103530. https://doi.org/10.1016/j.ijnonlinmec.2020.103530.

Kamenskiy, A., Seas, A., Bowen, G., Deegan, P., Desyatova, A., Bohlim, N., Poulson, W., Mactaggart, J., 2016. In situ longitudinal pre-stretch in the human femoropopliteal artery. Acta Biomat. 32, 231-237. http://doi.org/10.1016/j.actbio.2016.01.002.

Lopata, R. G. P., Nillesen, M. M., Hansen, H. H. G., Gerrits, I. H., Thijssen, J. M., de Korte, C. L. 2009. Performance evaluation of methods for two-dimensional displacement and strain estimation using ultrasound radio frequency data. Ultrasound Med. Biol. 35, 796-812. https://doi.org/:10.1016/j.ultrasmedbio.2008.11.002.

Mańkowski, J., Lipnicki, J., 2017. Digital materials - evaluation of the possibilities of using selected hyperelastic models to describe constitutive relations. Int. J. Appl. Mech. Eng. 22, 601-612. https://doi.org/10.1515/ijame-2017-0038.

Meng, L., Yang, X., Salcedo, E., Baek, D.-C., Ryu, J. E., Lu, Z., Zhang, J., 2020. A combined modeling and experimental study of tensile properties of additively manufactured polymeric composite materials. J. Mater. Eng. Perfor. 29, 2597-2604. http://doi.org/10.1007/s11665-020-04746-5.

Merodio, J., Ogden, R. W., 2016. Extension, inflation and torsion of a residually stressed circular cylindrical tube. Continuum. Mech. Therm. 28(1-2), 157-174. https://doi.org/10.1007/s00161-015-0411-z

Morris, K., Rosenkranz, A., Seibert, H., Ringel, L., Diebels, S., Talke, F. E., 2020. Uniaxial and biaxial testing of 3D printed hyperelastic photopolymers. J. Appl. Polym. Sci. 137, 48400. https://doi.org/10.1002/app.48400.

Ogden, R. W., 1972. Large deformation isotropic elasticity – on the correlation of theory and experiment for incompressible rubberlike solids. Proc. Math. Phys. Eng. Sci. 326, 565–584. https://doi.org/10.1098/rspa.1972.0026.

Ogden, R. W., 1997. Non-Linear elastic deformations. Dover Publications, Mineola.

Pagac, M., Schwarz, D., Petru, J., Polzer, S., 2020. 3D printed polyurethane exhibits isotropic elastic behavior despite its anisotropic surface. Rapid Prototyp. J. 26, 1371-1378. https://doi:10.1108/RPJ-02-2019-0027.

Ryu, J. E., Salcedo, E., Lee, H. J., Jang, S. J., Jang, E. Y., Yassi, H. A., Baek, D., Choi, D., Lee, E., 2019. Material models and finite analysis of additively printed polymer composites. J. Compos. Mater. 53, 361-371. https://doi.org/10.1177/0021998318785672.

Salman, H. E., Ramazanli, B., Yavuz, M. M., Yalcin, H. C., 2019. Biomechanical investigation of disturbed hemodynamics-induced tissue degeneration in abdominal aortic aneurysms using computational and experimental techniques. Front. Bioeng. Biotechnol. 7, 111. https://doi.org/:10.3389/fbioe.2019.111.

Schulze-Bauer, C. A. J., Mörth, C., Holzapfel, G. A., 2003. Passive biaxial mechanical response of aged human iliac arteries. J. Biomech. Engineering. 125, 395-406. https://doi.org/10.1115/1.1574331.

Slesarenko, V., Rudykh, S., 2018. Towards mechanical characterization of soft digital materials for multimaterial 3D-printing. Int. J. Eng. Sci. 123, 62-72. https://doi.org/10.1016/j.ijengsci.2017.11.011

Sommer, G., Regitnig, P., Költringer, L., Holzapfel, G. A., 2010. Biaxial mechanical properties of intact and layer-dissected human carotid arteries at physiological and supraphysiological loadings. Am. J. Physiol. - Heart Circ. Physiol. 298, 898-912. https://doi.org/10.1152/ajpheart.00378.2009.

Van Loon, P., Klip, W., Bradley, E. L., 1977. Length-force and volume-pressure relationships of arteries. Biorheology. 14, 181-201. http://doi.org/10.3233/BIR-1977-14405.

Wang, S., Guo, Z., Zhou, L., Li, L., Fu, Y., 2019. An experimental study of localized bulging in inflated cylindrical tubes guided by newly emerged analytical results. J. Mech. Phys. Solids, 124, 536-554. https://doi.org/10.1016/j.jmps.2018.11.011.